

Clump formation through colliding stellar winds in the Galactic Centre

D. Calderón^{1*}, A. Ballone^{2,3}, J. Cuadra¹, M. Schartmann⁴, A. Burkert^{2,3} and S. Gillessen²

¹*Instituto de Astrofísica, Facultad de Física, Pontificia Universidad Católica de Chile, 782-0436 Santiago, Chile*

²*Max Planck Institute for Extraterrestrial Physics, P.O. Box 1312, Giessenbachstr., D-85741 Garching, Germany*

³*Universitätssternwarte der Ludwig-Maximilians-Universität, Scheinerstr. 1, D-81679 München, Germany*

⁴*Centre for Astrophysics and Supercomputing, Swinburne University of Technology, Hawthorn, Victoria, 3122, Australia*

Draft 7 December 2024

ABSTRACT

The gas cloud G2 is currently being tidally disrupted by the Galactic Centre super-massive black hole, Sgr A*. The region around the black hole is populated by ~ 30 Wolf-Rayet stars, which produce strong outflows. We explore the possibility that gas clumps originate from the collision of stellar winds via the *non-linear thin shell instability*. We follow the thermal evolution of slabs formed at colliding symmetric winds, evaluate whether instabilities occur, and estimate the resulting clump masses. We find that the collision of relatively slow ($\lesssim 750 \text{ km s}^{-1}$) and strong ($\sim 10^{-5} \text{ M}_{\odot} \text{ yr}^{-1}$) stellar winds from stars at short separations ($\lesssim 1 \text{ mpc}$) is a process that indeed could produce clumps of G2’s mass and above. Encounters of single stars at such short separations are not common in the Galactic Centre, making this process a possible but unlikely origin for G2. We also discuss clump formation in close binaries such as IRS 16SW and in asymmetric encounters as promising alternatives that deserve further numerical study.

Key words:

1 INTRODUCTION

Gillessen et al (2012) detected a moving diffuse object, the so-called G2 cloud, on its way towards Sgr A*, the radio source identified as the central massive black hole of our Galaxy (see Genzel et al. 2010, for a review). The tidal disruption of this cloud is being monitored by different groups (e.g., Eckart et al. 2013; Gillessen et al. 2013; Phifer et al. 2013) and provides a unique opportunity to test accretion physics, due to both its proximity and the timescale on which it happens. Gillessen et al (2012) estimated the mass of G2 to be $\sim 3 \text{ M}_{\oplus}$ from its line emission. However, the nature of G2 has not been clarified yet. In particular, there is an ongoing debate on whether the diffuse cloud contains a compact mass (likely a star). Witzel et al. (2014) presented the detection of a compact source at $3.8 \text{ } \mu\text{m}$ (thermal dust emission) that would correspond to G2 during pericentre passage. Its survival as a compact source to the close passage ($\sim 2000 \text{ Schwarzschild radii}$) suggests the existence of a central star keeping it bound, which they argue is a binary merger product (Prodan et al. 2015). Other possible explanations for a central mass in G2 include an

evaporating proto-planetary disc or the wind of a T-Tauri star (Murray-Clay & Loeb 2012; Scoville & Burkert 2013; Ballone et al. 2013; De Colle et al. 2014).

On the other hand, Pfuhl et al. (2015) argued in favour of a purely gaseous cloud nature for G2 using their Brackett- γ observations. They interpreted this source as a bright knot of a larger gas streamer that includes a G2-type object called G1 in a similar orbit, but preceding it by 13 yr. G1 and G2 could be explained as the result of the partial tidal disruption of a star (Guillochon et al. 2014) or as one of many gas clumps created by the collision of stellar winds from the young stars in the Galactic centre (Burkert et al. 2012; Schartmann et al. 2012). Such dense, cold clumps are copiously produced in the SPH simulations of the Galactic centre gas dynamics performed by Cuadra et al. (2005, 2006, 2008, 2015) (see also Lützgendorf et al. 2015 § 3.3), and could survive pericentre passage if magnetised (McCourt et al. 2015). Moreover, G2’s orbit lies on the plane of the ‘clockwise disc’, defined by the orbits of many young stars (Paumard et al. 2006; Yelda et al. 2014), and its apocentre coincides with the inner rim of that disc. Nevertheless, the SPH technique has a tendency for artificially clumping gas (Hobbs et al. 2013), which raises doubts on how physical the clump formation is in such models. In this context, this work aims to test independently

* E-mail: dcaldero@astro.puc.cl

the clump formation as result of colliding stellar winds in the central parsec of the Milky Way.

Massive stars have significant phases of mass loss, in which their outflows are accelerated up to supersonic speeds due to radiation pressure. When two of these stars are at short separations, for example in a binary system, their winds collide and generate a hot slab of shocked gas. Depending on the ability of the gas in the slab to cool down, we will have different regimes. If the gas from both stars cools down rapidly, a cold thin shell will be produced centred at the contact discontinuity (hereafter CD) of the shocked gas interaction zone. This slab will be subject to strong instabilities such as the *Non-linear Thin Shell Instability* (hereafter NTSI, Vishniac 1994). In the case that only one of the winds is highly radiative, a cold thin shell will also be formed, but instabilities will be damped by the thermal pressure of the hot shocked gas from one of the stars (Vishniac 1983). When none of the winds are radiative, but there is a velocity difference between the winds, the Kelvin-Helmholtz instability (hereafter KHI) can be excited (Stevens et al. 1992; Pittard 2009). State-of-the-art numerical modelling of unstable colliding wind systems (Lamberts et al. 2011) highlights the high computational cost of realistic simulations of these systems. High spatial and time resolution are crucial to track the growth of instabilities. In this work we take an alternative approach and study the thermal evolution of the hot slab created from the winds collision, to predict under which conditions, out of a wide parameter space, the NTSI can grow; and estimate the possible resulting clump masses.

The paper is divided as follows, Section 2 describes the main cooling diagnostic we use through this work and Section 3 presents our model and the results of our parameter space study. Then, in Section 4 we discuss how likely is the formation of the G2 cloud through colliding winds based on our results. Finally, in Section 5 we present our conclusions and outlook.

2 RADIATIVE COOLING AND THIN SHELLS

Depending on their parameters, colliding winds have the ability to produce a dense, thin layer of cold gas. This slab can then be subject to different thin shell instabilities. In their numerical models, Stevens et al. (1992) identified such an instability that was the NTSI later described by Vishniac (1994), plus another damped instability consistent with the one described by Vishniac (1983). Moreover, Dgani et al. (1993) described another thin shell instability: the *Transverse Acceleration Instability* (TAI) that mainly takes place off the two-star axis. After detailed numerical modelling, Lamberts et al. (2011) concluded that the NTSI is the instability that dominates the slab evolution due to its large scale perturbations.

Whether the wind collision will produce a thin slab or not depends on how fast the shocked gas can be cooled down. Following the description presented in Stevens et al. (1992), the radiative efficiency of shocked stellar winds can be described by the *cooling parameter* χ , which is the ratio of the cooling timescale to the dynamical timescale,

$$\chi = \frac{t_{\text{cool}}}{t_{\text{dyn}}}, \quad (1)$$

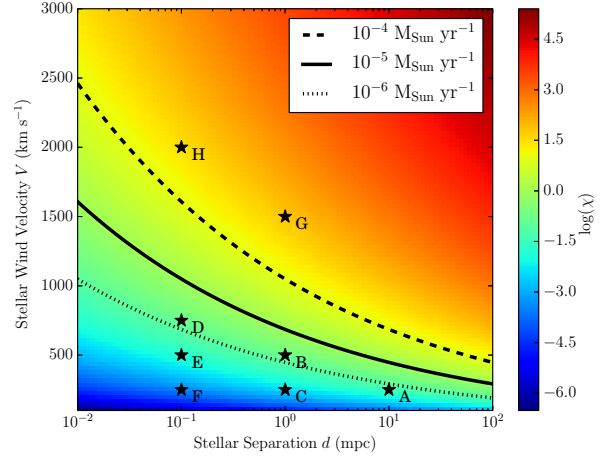


Figure 1. Cooling parameter as colour map on logarithmic scale which was obtained using Equation 3 and fixing the mass loss rate to $10^{-5} M_{\odot} \text{ yr}^{-1}$. It is shown as a function of the stellar separation d (for identical stars) on the x-axis and the stellar wind velocity V on the y-axis. The solid line shows $\chi = 1$ which separates the two regimes: adiabatic (above, $\chi > 1$) and roughly isothermal (below, $\chi < 1$) winds. Dashed and dotted lines show the $\chi = 1$ boundaries for mass loss rates of 10^{-4} and $10^{-6} M_{\odot} \text{ yr}^{-1}$, respectively. Black stars labelled A–H indicate the parameters of models we study in more detail in § 3. Notice that 1 mpc ~ 200 AU.

where t_{cool} and t_{dyn} are the cooling and the dynamical timescales, respectively. They are defined as,

$$t_{\text{cool}} = \frac{3k_{\text{B}}T}{2n\Lambda(T)}; \quad t_{\text{dyn}} = \frac{d_{*}}{c_{\text{s}}}, \quad (2)$$

where T and n are the temperature and number density of the shocked gas, respectively, $\Lambda(T)$ is the cooling function which we will specify in the following section, k_{B} is the Boltzmann constant, d_{*} is the distance between the star and the CD and c_{s} is the shocked gas sound speed. Therefore, for χ lower than unity, the gas can cool down faster through radiative cooling than through adiabatic expansion. On the contrary, χ larger than one means that radiative cooling is not efficient. Following Stevens et al. (1992), but using a cooling function that depends on temperature rather than being constant (see Equation 10), we can calculate the cooling parameter for each stellar wind given its properties,

$$\chi \approx \frac{1}{2} \frac{V_{\text{s}}^{5.4} d_{*12}}{\dot{M}_{-7}}, \quad (3)$$

where V_{s} is the terminal wind speed V in units of 1000 km s^{-1} , d_{*12} is the distance between the star and the CD d_{*} in units of 10^{12} cm and \dot{M}_{-7} is the mass loss rate \dot{M} in units of $10^{-7} M_{\odot} \text{ yr}^{-1}$. In Figure 1, we show χ as a function of V and the stellar separation of identical stars $d = 2d_{*}$ for $\dot{M} = 10^{-5} M_{\odot} \text{ yr}^{-1}$ fixed, which is the typical value for the Wolf-Rayet stars in the Galactic centre (see § 4). We have highlighted the boundary $\chi = 1$ to separate the two cooling regimes. We will concentrate on the $\chi < 1$ region, which is where the NTSI excitation is possible.

3 NTSI AND CLUMP FORMATION

As discussed in the previous section, if the slab gas cools down rapidly, different thin shell instabilities can be excited. The dominant instability is the NTSI, which is the result of the misalignment of the thermal pressure within the cold slab (which always acts perpendicular to the slab) and the ram pressure of the wind (always acting parallel to the wind direction). This generates a convergent flux onto perturbation knots where gas accumulates, and a subsequent mixing of both phases of the material. In this section we use the description of Vishniac (1994) to calculate the allowed wavelength range of the NTSI which can grow.

3.1 Range of unstable wavelengths

The growth of the NTSI can occur only for wavelengths shorter than those coordinated by sound waves: $\lambda < c_s t$. On the other hand, the shortest unstable wavelength is given by the slab thickness $l(t)$, i.e., $\lambda \gtrsim 2l(t)$. Moreover, the NTSI can grow only if the slab perturbation has an initial amplitude at least comparable to the thickness of the layer. Notice that the criteria depend on the time t elapsed since the formation of the slab.

The thickness of the slab generated by isothermal flows is given by $l(t) = 2V_n t$, where $V_n = V/(\mathcal{M}^2 - 1)$ is the velocity at which the slab thickens, $\mathcal{M} = V_s/c_s$ is the Mach number, and $V_s = V + V_n$ is the shock speed. Notice that for the limit of high Mach number $V_s \approx V$, and that the more supersonic the shock, the slower the slab increases its width.

3.2 Semi-analytical model

In our model we consider two identical stars that are fixed in space. They have a given mass loss rate and wind terminal velocity, and are separated by a given distance. Respectively, these three quantities \dot{M} , V and d , are the input parameters of the model. We follow the time evolution of the gas within the slab formed when the winds collide by studying its integrated density and thermal evolution, including a radiative cooling term. We define the relevant densities as,

$$\Sigma_{\text{slab}} = \rho_{\text{slab}} L, \quad (4)$$

where ρ_{slab} is the volumetric density inside the slab, Σ_{slab} is the surface density of the slab and L is the width of the slab. All these quantities evolve and we study them as a function of their age, i.e., the time after the wind collision. As we are studying a symmetric system (identical stars with identical winds), we model one side of the system. Therefore, $L(t)$ will be the distance from the CD to the discontinuity of the shocked and the free wind region. As the slab is supported by thermal pressure, in this point the thermal and the wind ram pressure have to be balanced, which is a reasonable assumption considering that the thermal energy is negligible in the free-wind region that is highly supersonic ($\mathcal{M} \gtrsim 20$). From this model, we can write the hydrodynamical equations as follows,

$$\frac{d}{dt} \Sigma_{\text{slab}} = \rho_{\text{wind}} V, \quad (5)$$

$$P_{\text{slab}} = \rho_{\text{wind}} V^2, \quad (6)$$

$$\frac{3k_B}{2\mu m_H} \frac{d}{dt} (\Sigma_{\text{slab}} T_{\text{slab}}) = H_{\text{shock}} + S_{\text{cool}}, \quad (7)$$

Table 1. Parameters of each model presented in this work. Column 1: Model name. Column 2: wind terminal velocity. Column 3: stellar separation. Column 4: cooling parameter χ estimated from Equation 3 and \dot{M} fixed to $10^{-5} M_\odot \text{ yr}^{-1}$.

Model	V (km s ⁻¹)	d (mpc)	χ
A	250	10.0	0.04
B	500	1.0	0.18
C	250	1.0	4.33×10^{-3}
D	750	0.1	0.16
E	500	0.1	0.02
F	250	0.1	4.33×10^{-4}
G	1500	1.0	69
H	2000	0.1	33

where P_{slab} is the pressure in the slab, μ is the mean molecular weight, m_H is the proton mass, H_{shock} is the mechanical heating term (i.e. kinetic energy flux from the wind per unit surface), and S_{cool} is the energy dissipation term through radiative cooling. These source terms are given by

$$H_{\text{shock}} = \frac{1}{2} \rho_{\text{wind}} V^3, \quad (8)$$

$$S_{\text{cool}} = \frac{\Sigma_{\text{slab}} \rho_{\text{slab}}}{\mu^2 m_H^2} \Lambda(T_{\text{slab}}), \quad (9)$$

where the cooling function $\Lambda(T)$ is an analytical approximation for optically thin radiative cooling for a metallicity of $3Z_\odot$ used by Cuadra et al. (2005, 2006, 2008, 2015) following Sutherland & Dopita (1993),

$$\Lambda(T) = 6.0 \times 10^{-23} \left(\frac{T}{10^7 \text{ K}} \right)^{-0.7} \text{ erg cm}^3 \text{ s}^{-1}. \quad (10)$$

Combining the system of Equations 5, 6, 7, 8, 9; and assuming an ideal gas $P_{\text{slab}} = \rho_{\text{slab}} k_B T_{\text{slab}} / (\mu m_H)$, we can derive a single differential equation that describes the thermal evolution of the slab:

$$\frac{3k_B}{2\mu m_H} \frac{d}{dt} T_{\text{slab}} = \frac{1}{2} \frac{V^2}{t} - \frac{\rho_{\text{wind}} V^2}{k_B \mu m_H} \frac{\Lambda(T_{\text{slab}})}{T_{\text{slab}}} - \frac{3k_B}{2\mu m_H} \frac{T_{\text{slab}}}{t}. \quad (11)$$

The first term on the right hand side represents the mechanical heating of the shock; the second, the radiative cooling; and the third, the work done by the slab. Furthermore, the slab density can be easily computed making use of Equation 6 and the ideal gas equation of state. Thus, the slab width time evolution can be calculated using Equations 4 and 5 to obtain

$$\frac{d}{dt} [\rho_{\text{slab}}(t) L(t)] = \rho_{\text{wind}} V \Rightarrow L(t) = \frac{\rho_{\text{wind}}}{\rho_{\text{slab}}(t)} V t. \quad (12)$$

From this expression we note that if the slab does not cool down (i.e. the slab density remains roughly constant), the slab will increase its width linearly with time; on the contrary, if the slab gets denser very rapidly it may overcome the linearity dependence with time and collapse as a thin shell which grows very slowly due to the fact that $\rho_{\text{wind}}/\rho_{\text{slab}} \ll 1$.

With this analysis we can calculate the NTSI growth criteria as a function of the age of the slab (or time after the wind collision). Although this model is very simple, it

provides us with information about the instabilities that can take place, the sizes and masses of the possible clumps.

3.3 Parameter study

Using the previously described procedure, we explored the parameter space shown in Figure 1. We first present in detail a few relevant and representative examples (see Table 1). In all these models we kept $\dot{M} = 10^{-5} \text{ M}_{\odot} \text{ yr}^{-1}$ fixed and stopped the calculation after the gas has cooled down significantly, reaching a temperature of 10^4 K . That is a reasonable temperature floor because of the presence of many hot, young stars emitting ionising radiation that prevents the temperature to drop to lower values¹.

The time evolution of the unstable wavelength criteria for the NTSI are shown for all models in Figures 2 and 3. Figure 2 shows the models with $\chi < 1$. Here, for most of the evolution of the slab, the upper limit (solid blue line) is *below* the lower limit (dashed green line), meaning that the instability cannot grow as there is no unstable wavelength range. Only at the very end of each calculation the upper limit is above the lower limit and therefore the instability develops. In these cases we registered the unstable length range and the final density values in Table 2. It is important to remark that for all these cases we remain in the thin shell regime, i.e., $L/d \ll 1$. Therefore we do not expect radiative cooling to be faster than the thermal response of the slab, making our assumption of pressure equilibrium at the shock valid.

Assuming spherical symmetry, we used the unstable wavelength range to compute a range of masses for clumps (see Table 2). From the results we see that larger stellar separations will result in larger clumps. However, these clumps are less dense due to the winds being significantly diluted before they collide. On the contrary, smaller separations produce smaller and denser clumps. The combination of these two factors sets the clump masses in a non-trivial manner. Our results show that *Model A*, *Model B* and *Model D* could generate clumps with masses $> 0.1 \text{ M}_{\oplus}$ and the most massive ones would be generated by *Model B*, reaching G2-like masses ($\sim 5 \text{ M}_{\oplus}$)².

On the other hand, Figure 3 shows the models with $\chi > 1$, in which we see that the width of the slab (dashed green line) becomes larger than the stellar separation (dotted red line) before there is an unstable wavelength range. Thus, we deem these models not physical, as our treatment cannot describe these systems properly, and we expect no clump formation through NTSI for this parameter range.

Although these results show that clump formation might occur for the $\chi < 1$ models, we need to check on which timescales this process takes place. Vishniac (1994) showed that the NTSI growth timescale τ is given by

$$\tau = \frac{\lambda^{1.5}}{\zeta^{0.5} c_s}, \quad (13)$$

where ζ is the initial amplitude of the perturbation. If we

assume $\zeta \sim \lambda$, the growth timescale is simply given by the sound crossing timescale, i.e., $\tau \sim \lambda/c_s$. Estimations of τ under this assumption for each of our models are presented in Table 2. Moreover, we present the clump masses as a function of the growth timescale for each model in Figure 4, where we see that models with shorter stellar separations ($d = 0.1 \text{ mpc}$ in green lines) tend to be the ones that can create clumps the quickest. This is due to these winds being less diluted when they collide, making the cooling more efficient. We can compensate this effect by increasing the wind speed, as a hotter slab would take longer to radiate most of its energy away. For example, comparing cases C and E (solid blue and dashed green, respectively) we see that the combination of different stellar separations and different wind speeds produces clump formation on roughly the same timescale.

An interesting point is that the models that can create the most massive clumps have significantly different parameters. This can be explained by the fact that clump masses are proportional to λ^3 , thus the most massive clump possibly generated would have a mass $M \propto \lambda_{\text{max}}^3$. Moreover, the upper limit of the unstable wavelength range of the NTSI is given by the sound crossing distance, i.e., $\int c_s dt$ integrated over the age of the slab when it reaches 10^4 K . This tells us that how massive clumps can be, depends on how long it takes for the slab to cool down and become unstable. Then, either high velocity winds and/or larger separations would produce more massive clumps. In order to illustrate this explicitly we have explored our parameter space more extensively, modelling 45 systems in total. We show this in Figure 5 as a function of the input parameters of our model. The left and right panels present the lower and upper limits of the clump mass range, respectively. Here it is easy to see that for larger separations and/or higher wind velocities the minimum and maximum clump masses are larger³.

To study which clumps will actually form, we take into account Equation 13 that shows that shorter wavelengths grow faster. Therefore for any model we would expect first the formation of the lightest possible clumps. On longer timescales, larger wavelengths would also act, accumulating the small clumps and possibly merging them to create more massive clumps. To actually predict a clump mass distribution, we require numerical simulations. We defer that study to a forthcoming work.

In general, we find that for parameters closer to $\chi = 1$ (black dashed line in Figure 5) we would expect more massive clumps to be formed. However we do not know exactly at what point our approach becomes unphysical as we go closer to the adiabatic regime, as seen in models G and H (see Figure 3). Thus, it is more sensible to explore the

³ We repeated the analysis for different mass loss rate values, 10^{-6} and $10^{-4} \text{ M}_{\odot} \text{ yr}^{-1}$, finding that for lower \dot{M} values, clumps can be more massive for the same combination of (d, V) , as a less dense slab makes the cooling less efficient, but we would need shorter distances and/or slower winds in order to get radiative winds in first place, as the $\chi = 1$ line moves down in the parameter space (see Figure 1). On the contrary, increasing \dot{M} we obtain less massive clumps for the same (d, V) , as a denser slab makes the cooling more efficient, but this would allow larger separations and/or faster winds to generate radiative winds, as the $\chi = 1$ line moves up in the parameter space.

¹ We also tested stopping the cooling at 10^5 K , finding that density values are systematically smaller by one order of magnitude.

² G2 could also have formed by mergers of smaller clumps, but we cannot address that option with our current approach.

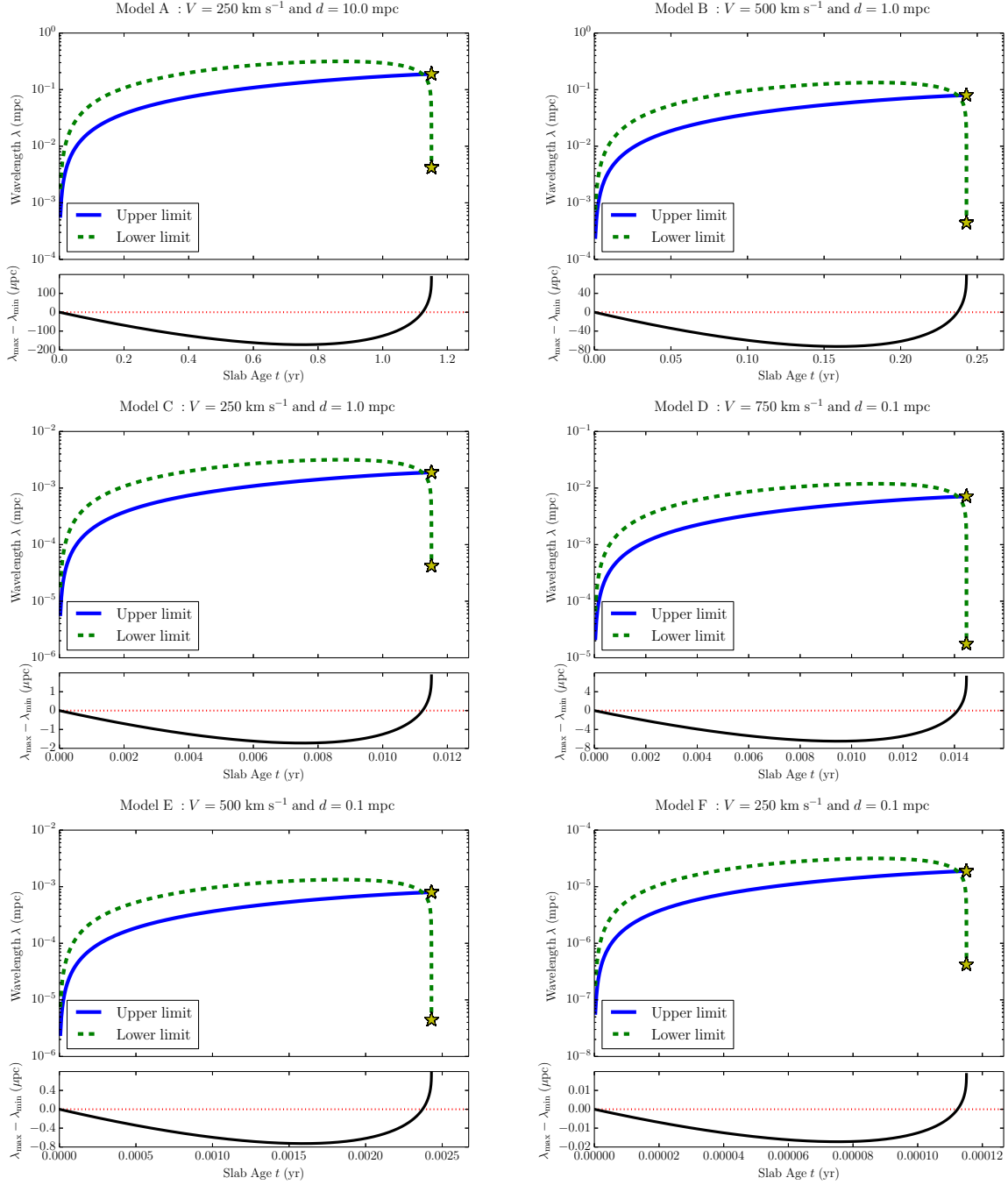


Figure 2. Evolution of the NTSI wavelength criteria for the radiative models ($\chi < 1$). On the upper panels we show the time evolution of the upper and lower limits of unstable wavelengths for the NTSI obtained from our semi-analytic prescription. Instabilities can grow only at the end of each time evolution, when a range of allowed wavelengths exists. Yellow stars represent the final state of the system when the gas has reached 10^4 K. On the lower panels, the thick black line represents the difference between the upper and lower limits, $\lambda_{max} - \lambda_{min}$, and the dotted red line is fixed at zero for reference. Note the different scales in the x- and y-axis between models.

parameter space close to $\chi = 1$ with numerical simulations. This is why we explored up to $\chi = 0.5$ only (black solid line). Despite this, we see that clump masses span a very wide range of masses and that the creation of clumps as massive as G2 is possible.

4 COLLIDING STELLAR WINDS IN THE GALACTIC CENTRE

We have studied the parameter space for close pairs of mass-losing stars, checking whether we expect them to form clumps through the NTSI, plus estimating the allowed range of sizes and masses for those clumps. Now, we apply this model to the stars in the central parsec of the Milky Way,

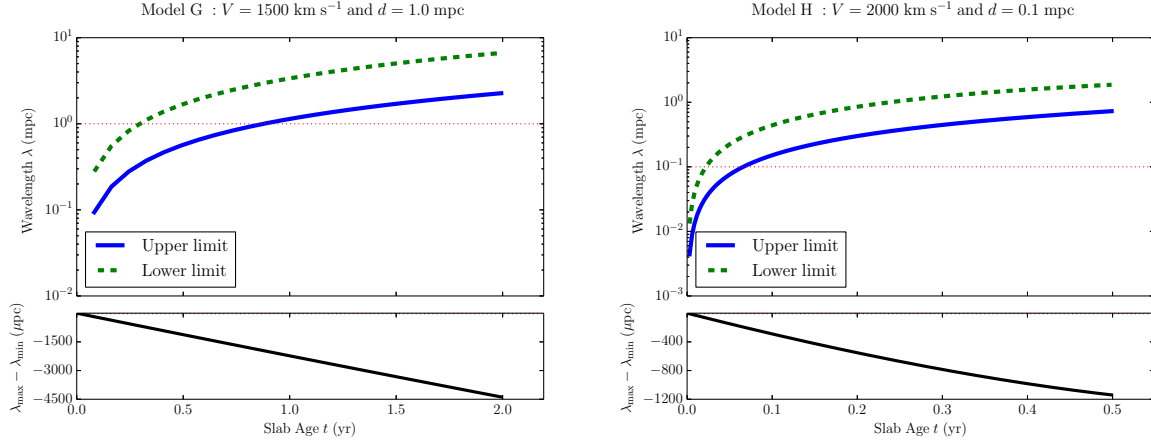


Figure 3. Same as Figure 2 but for the adiabatic models ($\chi > 1$) G and H. At some point the models become unphysical, as the slab width is comparable to the stellar separation (red dotted line). We do not expect NTSI excitation for these models.

Table 2. Results of our semi-analytic estimates for each model. Column 1: model name. Column 2: unstable wavelength range obtained from our analysis. Column 3: slab density obtained estimated from our calculations. Column 4: clump mass range computed assuming spherical clumps and uniform density with radius equal to the instability wavelengths. Column 5: growth timescale estimated assuming an initial amplitude equal to the instability wavelength and the slab sound speed at the temperature floor (10^4 K).

Model	Unstable λ (mpc)	ρ_{slab} (g cm $^{-3}$)	Clump Mass Range (M_{\oplus})	Growth Timescale (yr)
A	$(4 - 190) \times 10^{-3}$	2.4×10^{-18}	$3.6 \times 10^{-6} - 3.3 \times 10^{-1}$	$(3 - 120) \times 10^{-1}$
B	$(5 - 800) \times 10^{-4}$	4.7×10^{-16}	$8.8 \times 10^{-7} - 4.9 \times 10^0$	$(3 - 50) \times 10^{-1}$
C	$(4 - 190) \times 10^{-5}$	2.4×10^{-16}	$3.6 \times 10^{-10} - 3.3 \times 10^{-5}$	$(3 - 120) \times 10^{-3}$
D	$(2 - 710) \times 10^{-5}$	7.1×10^{-14}	$8.5 \times 10^{-9} - 5.3 \times 10^{-1}$	$(1 - 470) \times 10^{-3}$
E	$(5 - 800) \times 10^{-6}$	4.7×10^{-14}	$8.8 \times 10^{-11} - 4.7 \times 10^{-4}$	$(3 - 50) \times 10^{-4}$
F	$(4 - 190) \times 10^{-7}$	2.4×10^{-14}	$3.6 \times 10^{-14} - 3.3 \times 10^{-9}$	$(3 - 120) \times 10^{-5}$
G	-	2.6×10^{-19}	-	-
H	-	2.6×10^{-21}	-	-

as the NTSI could be excited for the colliding winds of young massive stars, and explain the origin of the G2 cloud. Our model assumes that the stars are stationary and that the pairs are identical. The first assumption is justified as the time-scales involved in the instability ($\lesssim 10$ yr, e.g., Figure 4) are typically much shorter than the duration of close stellar encounters of mass-losing stars in the Galactic Centre (see Table 4). The second issue is partially addressed in Section 4.3. Our sample of mass-losing stars in the inner parsec of the Galaxy is the same used in the numerical models by Cuadra et al. (2008, 2015) and it is listed in Table 3 including wind properties, which were taken from Martins et al. (2007) and Cuadra et al. (2008).

4.1 Radiative cooling diagnostic

We first estimate the critical separation between stars in order for their winds to be radiatively efficient. We use the previously defined *cooling parameter* χ , and compute the radiative-to-adiabatic transition separation equating $\chi = 1$,

$$d_*^{\text{cool}} = 2 \times 10^{12} \text{ cm} \frac{\dot{M}_{-7}}{v_{5.4}^{5.4}}. \quad (14)$$

Pairs of identical stars with separations $d > 2d_*^{\text{cool}}$ will produce adiabatic shocks, while those with $d < 2d_*^{\text{cool}}$ will

result in radiatively-cooled shocks. The value of $2d_*^{\text{cool}}$ is included in Table 3, and is also plotted as a function of the wind momentum fluxes in Figure 6. Note that, for any pair of stars, d changes with time as they orbit in the Galactic Centre, therefore colliding wind stars can go through both regimes. Star 33E has the largest value of d_*^{cool} . Encounters involving this star with similar ones at 10 mpc-scales should result in the formation of cold slabs. For the rest of the sample we see that only for separations below 0.1 – 1 mpc their winds would be radiatively efficient. Such short separations are in the range of close binary systems (Section 4.4).

4.2 Mass-losing stars encounters in the Galactic Centre

Now we turn our attention to the stellar orbits in the Galactic centre, to study how often close encounters between mass-losing stars are produced. To do so, we ran a simple, Newtonian gravity, test-particle simulation to follow the stars around Sgr A*. This approximation is correct, as the distances from the stars to Sgr A* are too large for relativistic effects to be important, and the time-scale for stellar scattering to be relevant is much longer than the period we are interested in (see Alexander 2005). We

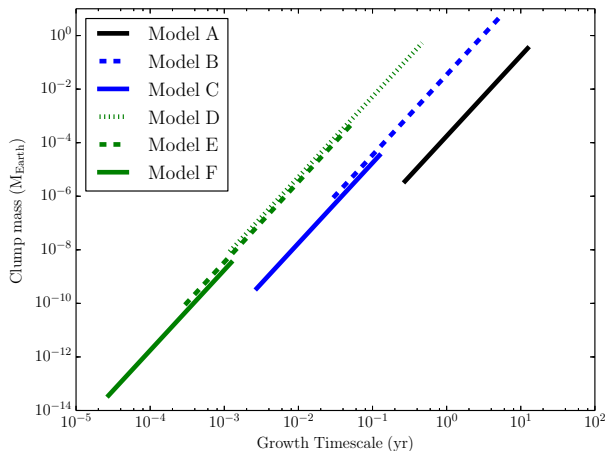


Figure 4. Clump masses (assuming spherical symmetry) generated through the NTSI, as a function of the instability growth timescale (assuming an initial amplitude comparable to the instability wavelength). Different stellar separations are shown with different colours: black, blue and green stand for 10, 1 and 0.1 mpc, respectively, while different wind velocities are shown with different line styles: solid, dashed and dotted represent 250, 500 and 750 km s⁻¹.

ran the models for 10⁴ yr, which is already a much longer timescale than the expected lifetime of a cloud like G2 (Burkert et al. 2012).

We only registered encounters of stellar pairs at distances shorter than 10 mpc based on our parameter space study, noting the minimum distance of the close passage d_{\min} and the duration of the encounter (i.e. the time stars are closer than 10 mpc). As initial conditions we used the 3D velocities and 2D sky positions observed by Paumard et al. (2006), meanwhile the unobservable z -coordinate was chosen using different assumptions for the orbital distribution. We used the 3 different models from the work by Cuadra et al. (2008) to obtain the z -coordinate of our young star sample: *Min-ecc*, *1Disc* and *2Discs*. *Min-ecc* uses the z -coordinate values that minimises the orbital eccentricities, *1Disc* assumes roughly half of the stars are in the well defined clockwise disc (Beloborodov et al. 2006), and *2Discs* assumes the existence of both clockwise and counter-clockwise discs. The results of this procedure are summarised in Table 4, where we see that over a 10⁴ yr period, at most there is one encounter with a ~ 1 mpc separation⁴. From the typical encounter duration of ~ 50 yr and our integration time, we can estimate a rough probability of producing G2 through encounters of single stars as 0.5%.

⁴ Notice that this “encounter” happens between stars 13E2 and 13E4, which might be bound together by a dark mass (Fritz et al. 2010), not included in our calculations. That dark mass would, however, likely increase the encounter duration.

Table 3. Galactic Centre mass-losing star sample taken from Martins et al. (2007) and Cuadra et al. (2008). Column 1: star ID. Column 2: star name. Both from Paumard et al. (2006). Column 3: stellar wind terminal velocity. Column 4: stellar mass loss rate. Column 5: twice the radiative-to-adiabatic wind transition distance computed from Equation 14.

ID	Name	V (km s ⁻¹)	\dot{M} (M _⊙ yr ⁻¹)	$2d_{*}^{\text{cool}}$ (mpc)
19	16NW	600	1.12×10^{-5}	2.29
20	16C	650	2.24×10^{-5}	2.97
23	16SW	600	1.12×10^{-5}	2.29
31	29N	1000	1.13×10^{-5}	0.15
32	16SE1	1000	1.13×10^{-5}	0.15
35	29NE1	1000	1.13×10^{-5}	0.15
39	16NE	650	2.24×10^{-5}	2.97
40	16SE2	2500	7.08×10^{-5}	0.01
41	33E	450	1.58×10^{-5}	15.28
48	13E4	2200	5.01×10^{-5}	0.01
51	13E2	750	4.47×10^{-5}	2.74
56	34W	650	1.32×10^{-5}	1.75
59	7SE	1000	1.26×10^{-5}	0.16
60	-	750	5.01×10^{-6}	0.31
61	34NW	750	5.01×10^{-6}	0.31
65	9W	1100	4.47×10^{-5}	0.35
66	7SW	900	2.00×10^{-5}	0.46
68	7W	1000	1.00×10^{-5}	0.13
70	7E2	900	1.58×10^{-5}	0.36
71	-	1000	1.13×10^{-5}	0.15
72	-	1000	1.13×10^{-5}	0.15
74	AFNW	800	3.16×10^{-5}	1.37
76	9SW	1000	1.13×10^{-5}	0.15
78	B1	1000	1.13×10^{-5}	0.15
79	AF	700	1.78×10^{-5}	1.58
80	9SE	1000	1.13×10^{-5}	0.15
81	AFNWNW	1800	1.12×10^{-4}	0.06
82	Blum	1000	1.13×10^{-5}	0.15
83	15SW	900	1.58×10^{-5}	0.36
88	15NE	800	2.00×10^{-5}	0.87

4.3 Asymmetric mass losing stars encounters

For simplicity, we have only analysed collisions of identical stellar winds. However, in reality we will typically have encounters between stars with different wind properties. To study such cases, detailed numerical simulations are needed, such as those performed by Lamberts et al. (2011). These authors have shown that even a small velocity difference in the colliding winds can excite the KHI. This would mix two-phase material on top of other instabilities that can take place simultaneously. Although all these processes can be very complicated to track analytically, based on our work we can give a qualitative description of possible scenarios that can take place for asymmetric close encounters.

Stellar wind encounters are characterised by their momentum flux ratio (Lebedev & Myasnikov 1990),

$$\eta = \frac{\dot{M}_2 V_2}{\dot{M}_1 V_1}, \quad (15)$$

where the subscript 2 stands for the weaker wind and 1 for the stronger one, so $\eta \leq 1$ by definition. For $\eta \neq 1$, the interaction zone of the shocked gas bends towards the weaker star. The CD distance to the weaker wind star will

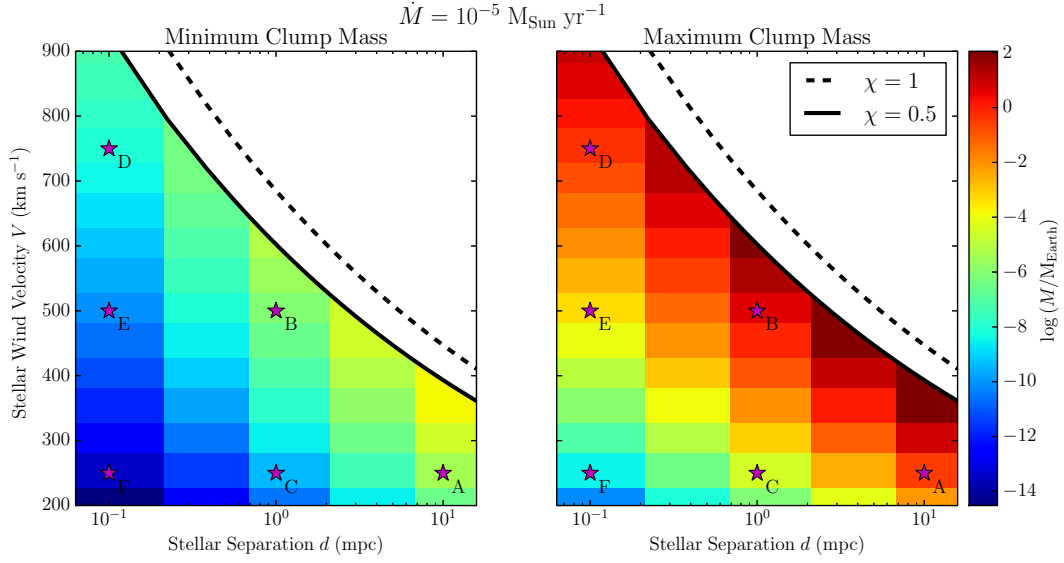


Figure 5. Parameter space (d, V) with $\dot{M} = 10^{-5} M_{\odot} \text{ yr}^{-1}$ fixed, displaying clump masses (colours) formed through NTSI obtained with our model. The left and right panels show the minimum (lower limit) and maximum (upper limit) clump mass for a given combination of parameters, respectively. Magenta star symbols show the models we previously studied in detail. The solid and dashed black lines stand for $\chi = 0.5$ and $\chi = 1$, respectively.

Table 4. Galactic Centre mass-losing star encounters at < 10 mpc. Column 1: initial conditions model name. Column 2: IDs of the stars in the encounter. For each pair, the asterisk symbol (*) marks the star with the weaker wind (i.e., smaller momentum flux). When no asterisk is shown, both stars have the same momentum flux. Column 3: minimum stellar separation in the encounter. Column 4: time stars are closer than 10 mpc. Column 5: wind momentum flux ratio estimated from Equation 15. Column 6: CD distance to the weaker wind star calculated from Equation 16. Column 7: weaker wind cooling parameter obtained from Equation 17. Column 8: whether the weaker wind is radiative or not at the minimum stellar separation of the encounter.

Model	Stars	d_{\min} (mpc)	Duration (yr)	η	R_2 (mpc)	Weaker wind χ_{asym}	Thin shell? ($\chi_{\text{asym}} < 1$)
<i>1Disc</i>							
	40 – 60*	9.2	10	0.021	1.164	7.581	NO
	48 – 60*	4.0	80	0.034	0.622	4.052	NO
	48 – 51*	1.0	1200	0.304	0.355	0.260	YES
	51 – 60*	6.0	70	0.112	1.504	9.797	NO
<i>2Discs</i>							
	19* – 48	3.0	15	0.061	0.594	0.519	YES
	19* – 51	7.0	20	0.200	2.163	1.889	NO
	19* – 48	2.0	220	0.061	0.396	0.347	YES
	19* – 51	4.0	20	0.200	1.236	1.080	NO
	19* – 51	9.5	10	0.200	2.936	2.564	NO
	20 – 32*	8.0	60	0.776	3.747	51.158	NO
	31 – 72	7.5	20	1.000	3.750	51.200	NO
	39* – 51	2.0	15	0.434	0.794	0.534	YES
	41* – 48	9.0	10	0.065	1.828	0.240	YES
	48 – 51*	5.0	550	0.304	1.777	1.297	NO
<i>Min-ecc</i>							
	23* – 41	8.0	50	0.945	3.943	3.442	NO
	48 – 51*	1.0	1200	0.304	0.355	0.260	YES
	48 – 60*	4.0	80	0.034	0.623	4.058	NO
	48 – 61*	6.0	20	0.034	0.934	6.084	NO
	51 – 60*	6.0	70	0.112	1.504	9.797	NO
	51 – 61*	7.5	25	0.112	1.881	12.252	NO

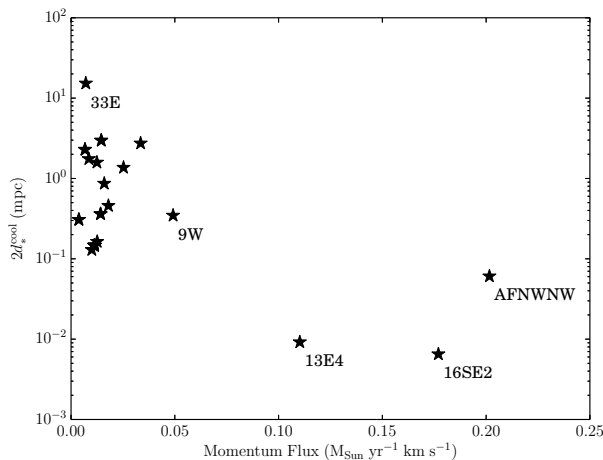


Figure 6. Critical stellar separation in order for their winds to be efficiently radiative (i.e. their collision could produce a *thin shell*) as a function of their wind momentum flux ($\dot{M} \times V$). The sample plotted corresponds to the one shown in Table 3. Stars with large momentum fluxes are labelled, as they can be important in asymmetric encounters “forcing” weaker winds to radiate their energy rapidly, resulting in radiative shocks. Star 33E is also labelled as it has the largest value of d_*^{cool} .

be given by

$$R_2 = \frac{\sqrt{\eta}}{1 + \sqrt{\eta}} d. \quad (16)$$

Then, smaller η will move the CD closer to the weaker star, producing a denser slab. In Figure 6, we highlighted the stars with largest momentum fluxes in their winds, including their names on the plot. Encounters of these stars with others, of the left side of the plot, will produce encounters with small η and short distances R_2 from the weaker star to the CD. For each of the encounters we registered in the previous subsection, we calculated the momentum flux ratio and the R_2 value. We can now modify the definition of the cooling parameter (Equation 3), so it uses the distance R_2 at which the CD is expected to form in the asymmetric close encounters,

$$\chi_{\text{asym}} \approx \frac{1}{2} \frac{V_{8.4}^{5.4} R_{2,12}}{\dot{M}_{-7}}, \quad (17)$$

where $R_{2,12} = R_2/10^{12}$ cm. Since R_2 is always a fraction of $d/2$, the density of the weaker wind will be higher at that position compared to the symmetric case and the slab will be able to radiate its energy away more rapidly. All these estimates are included in Table 4. From those results we can check that for two of our models (*1Disc* and *Min-ecc*) there is only one encounter where the weaker wind produces a cold slab that might become unstable, while in the other case (*2Discs*), there are four such encounters. The difference is at least partially due to the fact that in the *2Discs* case the stars are closer together and more encounters are produced in general. These systems deserve more study because they could be clump sources.

It is important to remark that, in the asymmetric case, on one side of the CD we have a thin shell while on the other

we have the hot shocked gas of the stronger wind. The latter tends to stabilise any instability possibly excited, so even if $\chi_{\text{asym}} < 1$ there might be no clump formation. Also notice that all these estimates were done under the assumption that the stars are separated well enough in order to accelerate their winds up to their terminal velocities. However, for extreme values of η that might not be the case.

4.4 Binary stars

As shown in Section 4.1, the formation of cold slabs typically requires stellar separations below 1 mpc. While those separations are not often achieved in stellar encounters of single stars, they are easily fulfilled by close binaries. The census of young massive binary stars in the Galactic Centre is still incomplete, but the recent study by Pfuhl et al. (2014) increased to three the amount of confirmed binary systems: (i) IRS 16SW, a 19.5-day period Ofpe/WN9 eclipsing contact binary (Martins et al. 2006), (ii) IRS 16NE, a 224-day period Ofpe/WN9 binary and (iii) E60⁵, a 2.3-day eclipsing contact Wolf-Rayet binary. The inferred separations of these binary systems are of the order of 10 μ pc and below. That, together with the wind properties listed in Table 3, could make these three binaries very effective sites for clump formation. IRS 16SW is of particular interest, as it has a clockwise orbit that roughly coincided with G2’s at the latter’s apocentre. Notice that the wind properties of these stars were assigned by Cuadra et al. (2008) based on their similarity to other stars whose spectra were properly modelled by Martins et al. (2007). However, we would not expect any important wind component to be substantially faster, as it would show up as broader lines in the spectra. Additionally, from the estimations by Pfuhl et al. (2014) we expect an overall $\sim 30\%$ spectroscopic binary fraction for the massive OB/WR stars in the Galactic Centre. Thus, even though our current knowledge of the binary population in the Galactic Centre is limited, close binary systems remain as a very promising possibility for the creation of cold clumps. A more detailed numerical model of this process is deferred to a forthcoming paper.

5 CONCLUSIONS

We have developed a simple and straightforward prescription to study clump formation through the NTSI mechanism in symmetric colliding wind systems. The input parameters are the mass loss rate, wind terminal velocity and stellar separation. Radiatively efficient wind collisions are capable of creating cold gas clumps (10^4 K) in a wide range of masses, where the most massive ones are of the order of the Earth mass for strong outflows $\dot{M} = 10^{-5} M_{\odot} \text{ yr}^{-1}$, relatively slow wind terminal velocities 250 – 750 km s^{-1} and short stellar separations 0.1 – 1 mpc. Nevertheless, the wide range of unstable wavelengths that are excited prevents us from predicting unequivocal clump masses, as shorter-wavelength perturbations grow faster and might hinder the development of larger-scale ones.

We also found that the possible clump masses depend

⁵ The star with ID 60 in Table 3.

strongly on the timescale needed for the slab to collapse within the radiative wind regime. The most massive ones would be generated in systems where the shocked gas does not cool instantaneously, i.e. systems with χ approaching unity. Studying that regime however is not straightforward as both radiative and adiabatic cooling are important.

Our results show that the formation of gas clumps with masses comparable to the G2 cloud is indeed possible in symmetric colliding winds. However, this scenario does not seem likely in the Galactic Centre given the currently known mass-losing star sample, as the required sub-mpc separations are very rarely achieved by them. We also discussed clump formation in asymmetric encounters, finding that the massive and slow outflow of IRS 33E could create clumps if confined by a powerful wind of another star. Similarly, the collision of winds from IRS 13E2 and 13E4 could also generate a cold slab unstable to the NTSI. These stars have similar orbits and spend a significant time at short separations, which could explain the presence of many dusty clumps in their vicinity (see [Fritz et al. 2010](#)). However, they orbit Sgr A* in the opposite sense as G2, making this pair an unlikely origin for this particular cloud. An promising possibility is that clumps are produced in close binaries, of which three are currently known. Still, better observational data are required to constrain the wind properties of both components of each binary. The IRS 16SW binary is of particular interest, as its orbit coincides with G2's at apocentre.

In conclusion, given our current analysis and the available stellar wind data, the formation of G2-like clouds in the Galactic centre appears as a possible but not very common event. We defer more concrete results to a future study using 2D and 3D numerical modelling. That is required to treat systems with unequal stellar winds, with $\chi \sim 1$, or for winds that collide before reaching their terminal velocity, such as compact binaries. Numerical models are also required to follow the growth of different unstable wavelength and obtain a clump mass function.

ACKNOWLEDGMENTS

We thank Cristian Hernández for checking some of the calculations. Part of this work was carried out at MPE, which DC and JC thank for the warm hospitality. We acknowledge support from CONICYT-Chile through FONDECYT (1141175), Basal (PFB0609) and Anillo (ACT1101) grants. DC is supported by CONICYT-PCHA Magíster Nacional (2013-22130903) and PCHA/Doctorado Nacional (2015-21151574). AB was supported by the Deutsche Forschungsgemeinschaft (DFG) priority program 1573 (Physics of the Interstellar Medium) and by the DFG Cluster of Excellence “Origin and Structure of the Universe”.

REFERENCES

Alexander, T. 2005, *PhysRep*, 419, 65
 Ballone, A., Schartmann, M., Burkert, A. et al. 2013, *ApJ*, 776, 13
 Boloborodov, A. M., Levin, Y., Eisenhauer, F. et al. 2006, *ApJ*, 648, 405

Blondin, J. M., Kallman, T. R., Fryxell, B. A. et al. 1990, *ApJ*, 356, 591
 Burkert, A., Schartmann, M., Alig, C. et al. 2012, *ApJ*, 750, 58
 Colella, P. & Woodward, P. R., 1984, *JCoPh*, 54, 174
 Cuadra, J., Nayakshin, S., Springel, V. et al. 2005, *MNRAS*, 360, L55
 Cuadra, J., Nayakshin, S., Springel, V. et al. 2006, *MNRAS*, 366, 358
 Cuadra, J., Nayakshin, S. & Martins, F. 2008, *MNRAS*, 383, 458
 Cuadra, J., Nayakshin, S. & Wang, Q. D. 2015, *MNRAS*, 450, 277
 De Colle, F., Raga, A. C., Contreras-Torres, F. F. et al. 2014, *ApJL*, 789, L33
 Dgani, R., Walder, R. & Nussbaumer, H. 1993, *A&A*, 267, 155
 Eckart, A., Mužić, K., Yazici, S., et al. 2013, *A&A*, 551, A18
 Fritz, T. K., Gillessen, S., Dodds-Eden, K. et al. 2010, *ApJ*, 721, 395
 Genzel, R., Eisenhauer, F., & Gillessen, S. 2010, *Reviews of Modern Physics*, 82, 3121
 Gillessen, S., Genzel, R., Fritz, T. K. et al. 2012, *Nature*, 481, 51
 Gillessen, S., Genzel, R., Fritz, T. K. et al. 2013, *ApJ*, 763, 78
 Guillochon, J., Loeb, A., MacLeod, M. et al. 2014, *ApJL*, 786, L12
 Hobbs, A., Read, J., Power, C. & Cole, D. 2013, *MNRAS*, 434, 1849
 Lamberts, A., Fromang, S. & Dubus, G. 2011, *MNRAS*, 418, 2618
 Lebedev M. G., Myasnikov A. V., 1990, *Fluid Dynamics*, 25, 629
 Lützgendorf, N., Kissler-Patig, M., Gebhardt, K. et al. 2015, *arXiv:1501.07441*
 Martins, F., Trippe, S., Paumard, T., et al. 2006, *ApJ*, 649, L103
 Martins, F., Genzel, R., Hillier, D. J. et al. 2007, *A&A*, 468, 233
 McCourt, M., O’Leary, R. M., Madigan, A.-M., & Quataert, E. 2015, *MNRAS*, 449, 2
 Murray-Clay, R. A., & Loeb, A., 2012, *Nat. Commun*, 3, 1049
 Paumard, T., Genzel, R., Martins, F. et al. 2006, *ApJ*, 643, 1011
 Phifer, K., Do, T., Meyer, L., et al. 2013, *ApJ*, 773, L13
 Pfuhl, O., Alexander, T., Gillessen, S. et al. 2014, *ApJ*, 782, 101
 Pfuhl, O., Gillessen, S., Eisenhauer, F. et al. 2015, *ApJ*, 798, 111
 Pittard, J. M. 2009, *MNRAS*, 396, 1743
 Pittard, J. M. 2011, *BSRSL*, 80, 555
 Prodan, S., Antonini, F. & Perets, H. B. 2015, *ApJ*, 799, 118
 Scoville, N., & Burkert, A. 2013, *ApJ*, 768, 108
 Schartmann, M., Burkert, A., Alig, C. et al. 2012, *ApJ*, 708, 605
 Stevens, I. R., Blondin, J. M. & Pollock, A. M. 1992, *ApJ*, 386, 265
 Sutherland, R. S. & Dopita, M. A. 1993, *ApJS*, 88, 253
 Vishniac, E. T. 1983, *ApJ*, 274, 152
 Vishniac, E. T. 1994, *ApJ*, 428, 186
 Witzel, G., Ghez, A. M., Morris, M. R. et al. 2014, *ApJ*, 796, 8
 Yelda, S., Ghez, A. M., Lu, J. R., et al. 2014, *ApJ*, 783, 131